

High Temperature Reduction of Bauxite Residue [†]

Lanjar Grahita, Zulfiadi Zulhan and Taufiq Hidayat * 

Metallurgical Engineering Research Group, Faculty of Mining and Petroleum Engineering, Institut Teknologi Bandung, Bandung 40132, Indonesia; lanjar1708@gmail.com (L.G.); zulfiadi.zulhan@gmail.com (Z.Z.)

* Correspondence: t.hidayat@itb.ac.id

[†] Presented at International Conference on Raw Materials and Circular Economy, Athens, Greece, 5–9 September 2021.

Abstract: The present study focused on investigating the high-temperature reduction of bauxite residue, also known as red mud. A series of reduction experiments on red mud was performed to investigate the influences of temperature (1400, 1450, and 1500 °C), reaction time (15, 30, and 60 min) and reductant addition (7 and 14% carbon). A reduction experiment using a combination of carbon and plastic in the form of linear low-density polyethylene (7% carbon and 5% LLDPE) was also tested. The experiments were carried out in a vertical tube furnace using a graphite crucible under an argon atmosphere. Phases formed after the reduction process was analyzed using a scanning electron microscope equipped with an energy dispersive spectroscopy detector. At 7% carbon addition for all reduction temperatures and times, the reduction process of red mud produced metal and slag. The metal mainly consisted of iron with main trace elements of Si, Ti, P, S, and V. The slag mainly consisted of Na₂O, Al₂O₃, SiO₂, CaO, and TiO₂ components with residual iron oxide of less than 3.5 wt.%. Increasing the carbon addition to 14% at 1450 °C significantly increased the Si content in metal up to 19.1 wt.% and significantly decreased Na₂O in slag to less than 0.1 wt.%. The experiment with 7% carbon + 5% LLDPE addition gave a similar reduction extent to the experiment with only 7% carbon addition. The combustion of the LLDPE occurred before the reduction took place, and hence the LLDPE did not significantly contribute to the reduction process.

Keywords: bauxite residue; red mud; high temperature reduction; metal-slag equilibrium



Citation: Grahita, L.; Zulhan, Z.; Hidayat, T. High Temperature Reduction of Bauxite Residue. *Mater. Proc.* **2021**, *5*, 128. <https://doi.org/10.3390/materproc2021005128>

Academic Editor: Anthimos Xenidis

Published: 14 April 2022

Publisher's Note: MDPI stays neutral with regard to jurisdictional claims in published maps and institutional affiliations.



Copyright: © 2022 by the authors. Licensee MDPI, Basel, Switzerland. This article is an open access article distributed under the terms and conditions of the Creative Commons Attribution (CC BY) license (<https://creativecommons.org/licenses/by/4.0/>).

1. Introduction

Bauxite residue or red mud is a waste generated from the processing of bauxite into alumina through the Bayer process [1]. The quantity of red mud produced for every ton of alumina production is significant, and thus the storage of red mud is a challenge for alumina producers. Red mud storage pond dams sometimes collapse or fail due to heavy rains that cause flooding and breaching, posing a threatening environmental problem and safety issues. The utilization of red mud is one of the solutions that can minimize environmental and safety risks associated with red mud storage.

There are different themes of research on red mud utilization, one of which is research on the high-temperature reduction of red mud to produce metallic iron [2–10]. However, there is limited publication reporting research on the high-temperature reduction of Indonesian red mud, which has a higher Al₂O₃/Fe₂O₃ ratio and a lower TiO₂ content than those in red muds of different origins reported in the literature [5,11–16].

This research aims to study the high-temperature reduction of Indonesian red mud. Thermodynamic evaluation has been carried out to understand the chemistry of the process. A series of laboratory-scale experiments have been performed using a vertical furnace to evaluate the reducibility of the red mud and the composition of phases formed by the reduction process.

2. Materials and Methods

The red mud used in this study is from Tayan, West Kalimantan, Indonesia. The red mud was ground and screened to obtain red mud particles with size less than 65 microns. The red mud was characterized using X-ray fluorescence (XRF, Rigaku WDXRF Supermini 200) and X-ray powder diffraction (XRD, Rigaku Smartlab SE) to determine its chemical composition and mineralogy. The XRF measured composition of red mud is provided in Table 1; each element was recalculated to a selected oxidation state. The red mud contained dominantly iron oxide, alumina, silica, and sodium oxide. XRD analysis in Figure 1 indicates the presence of hematite, gibbsite, quartz, calcite, goethite, and sodalite minerals in the red mud. Carbon powder (<100 μm) was used as a reductant. Using plastic material as reductant material to partially substitute the carbon powder was also tested by combining carbon powder and linear low-density polyethylene (LLDPE) in one of the experiments.

Table 1. Composition of red mud based on XRF analysis (wt.%).

Fe_2O_3	Al_2O_3	SiO_2	CaO	Na_2O	TiO_2	V_2O_5	Sc_2O_3	SO_3	LOI
30.9	23.2	15.4	3.6	8.9	2.3	0.17	0.006	0.40	14.4

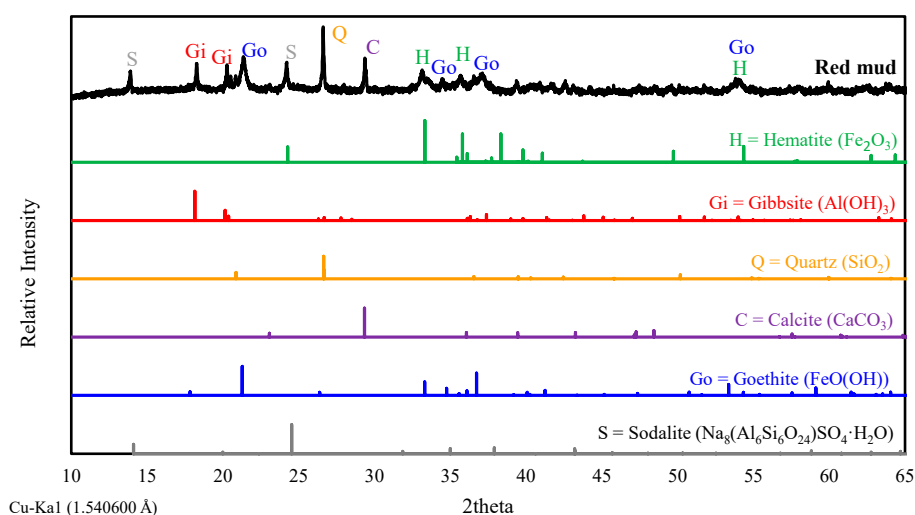


Figure 1. X-ray diffraction pattern of red mud.

Thermodynamic analysis of the process was then performed using the red mud composition and mineralogy data. The thermodynamic aspect of the high-temperature processing of red mud has been analyzed by performing calculations using FactSage thermochemical software version 7.3 (CRCT-ThermFact Inc, Canada & GTT-Technologies, Aachen, Germany). FactSage is equipped with the most integrated databases in the field of thermochemistry. The FactSage databases contain all parameters of Gibbs energies for elements, compounds, and solutions in the gas, solid, and liquid phases. By defining the input parameters, the amount and composition of phases from a chemical process can be predicted by FactSage.

A series of lab-scale experiments in a vertical tube furnace was also carried out to investigate the actual reducibility of the red mud and the composition of phases formed after the high-temperature reduction process. The vertical tube furnace consisted of an alumina tube held by holders made of stainless steel. The tube was placed inside the vertical furnace and was electrically heated. A B-type thermocouple was installed inside the tube to accurately monitor the temperature around the sample during the reduction process. The total weight of red mud, carbon, and LLDPE mixture used in each experiment were less than 2 grams. The mixture was placed in a graphite crucible with 25 mm-OD.

The sample in the crucible was inserted from the bottom of the furnace and was suspended using a platinum wire hook. The bottom of the furnace was then sealed by submerging it in water inside a bucket to eliminate air ingress from the surrounding atmosphere. An inert atmosphere inside the alumina tube was achieved by introducing argon gas. After the inside of the alumina tube was completely filled with argon, the sample in the crucible was lifted into the hot zone of the furnace. Different experimental parameters were tested which included temperature (1400, 1450 and 1500 °C), time (15, 30 and 60 min), carbon addition (7 and 14% (g-carbon/g-red mud) = 1 and 2 × stoichiometrical requirement for iron oxide reduction in the red mud), and LLDPE addition (0 and 5% (g-LLDPE/g-red mud) = 0 and 1 × stoichiometrical requirement, assuming the LLDPE is composed of 100% C₂H₄).

After each experiment, the sample was rapidly quenched by dropping the sample into the water to preserve phases formed at high temperatures. The quenched sample was dried, mounted in epoxy resin, and sectioned using a semi-automatic polishing machine. The polishing quality was checked using an optical metallurgical microscope. The microscopic detail inside the reduction product was then examined using a scanning electron microscope (SEM, JEOL JSM-6510A, Tokyo, Japan) with a secondary electron (SE) detector. The compositions of phases inside the reduction product were also analyzed semi-quantitatively using an energy dispersive x-ray spectroscopy (EDS) detector installed within the SEM.

3. Results and Discussion

3.1. Thermodynamic Analysis

The thermodynamic aspects of high-temperature processing of red mud were evaluated using FactSage thermochemical software with an initial mixture having a ratio of 7% carbon + 5% LLDPE addition. The temperature of the calculation varied from 300 to 2000 °C. FTmisc database was selected for the solid and liquid iron solutions. FToxid database was selected for molten slag and solid oxide solutions, such as spinel ((Fe,Al)₃O₄) and nepheline ((Na,K)AlSiO₄). FactPS database was also selected for gas, pure elements, and stoichiometric compounds. The FactSage calculation showed that the red mud thermodynamically could be processed at high temperatures to produce metallic products. The calculation also provided information on the type and proportion of phases formed during the red mud's high-temperature processing, as shown in Figure 2. The calculation result shows that the dominant phases are spinel, nepheline, and Na₂Ca₃Al₁₆O₂₈ at low temperatures (300 °C). The spinel is reduced into solid iron starting from approximately 600 °C. The solid iron will melt to liquid iron above 1300 °C, while nepheline, Na₂Ca₃Al₁₆O₂₈, and other oxide components will completely melt into molten slag above 1250 °C.

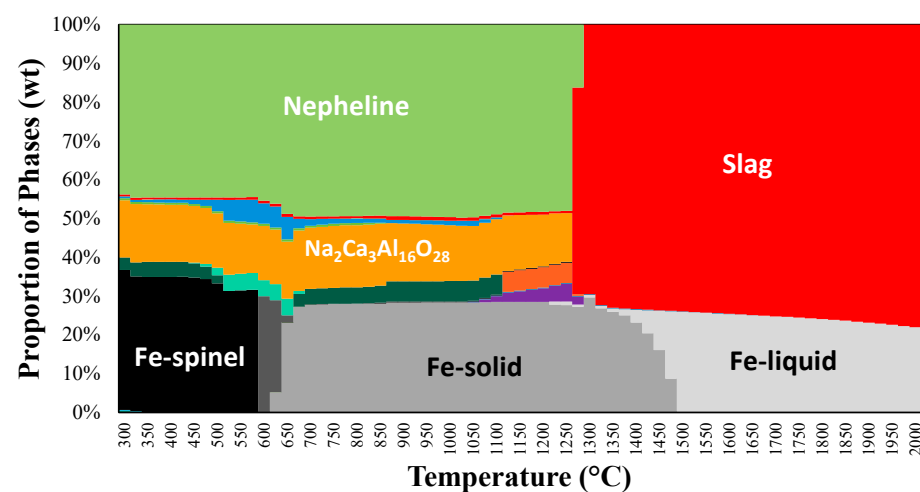


Figure 2. Type and proportion of phases as a function of temperature from reduction at 7% carbon + 5% LLDPE addition based on FactSage calculation.

3.2. Laboratory Scale Experimentation

Laboratory scale experiments using a vertical furnace at different temperatures, reaction times, carbon additions, and LLDPE additions have been performed. The SEM microstructures for selected samples are shown in Figure 3. Figure 3a shows the microstructure of the sample from the experiment at $T = 1450\text{ }^{\circ}\text{C}$ and $t = 60$ minutes with 7% carbon addition. Figure 3b shows the sample's microstructure from an experiment at $T = 1450\text{ }^{\circ}\text{C}$ and $t = 60$ minutes with 14% carbon addition. While Figure 3c shows the microstructure of sample from experiment at $T = 1450\text{ }^{\circ}\text{C}$ and $t = 60$ min with 7% carbon + 5% LLDPE addition. All microstructures show the formation of the metal phase and slag phase. The only difference was the sample from the reduction with 14% carbon addition, where the formation of solid Al_2O_3 was observed (Figure 3b).

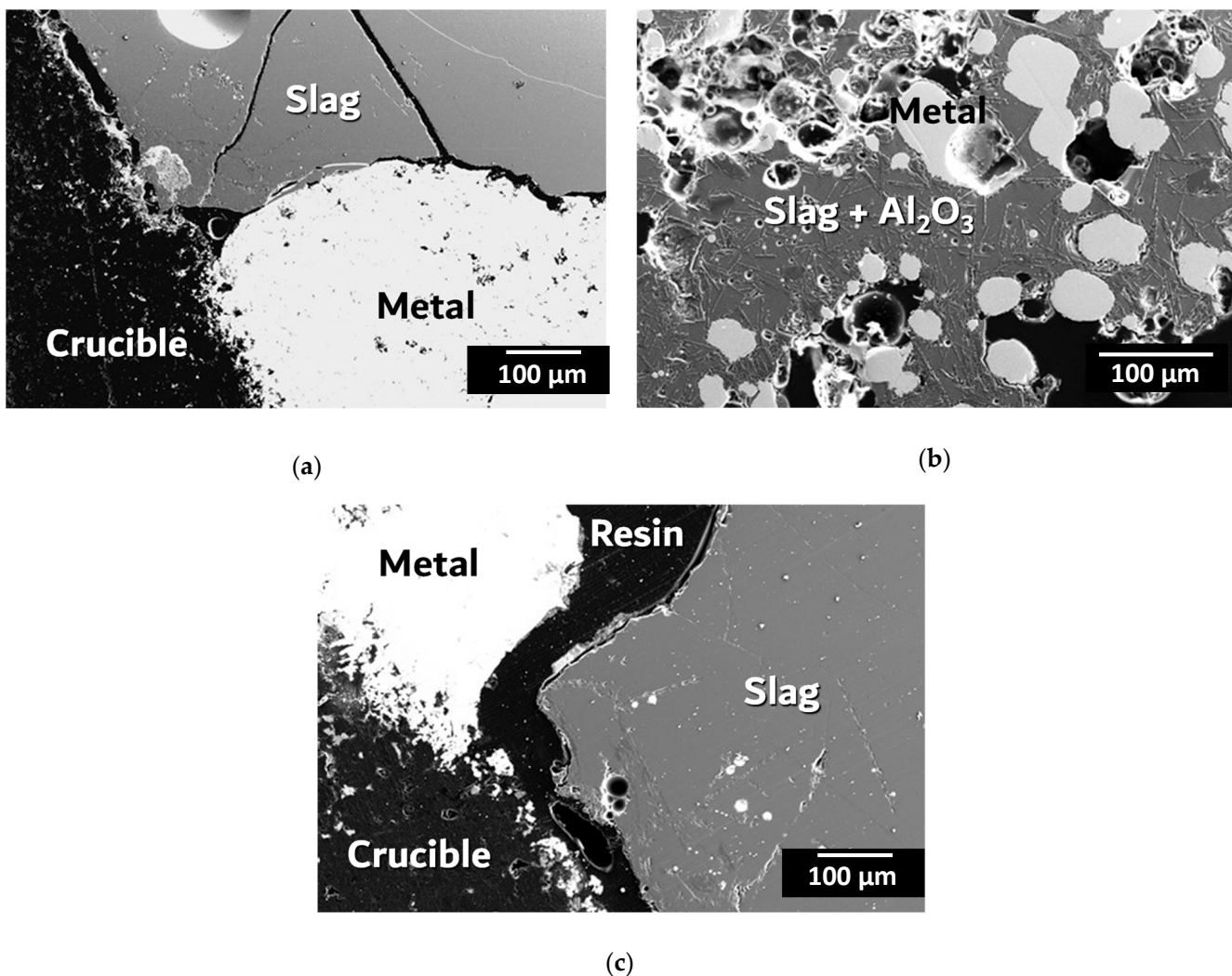


Figure 3. Microstructures of quenched samples from experiments at $T = 1450\text{ }^{\circ}\text{C}$ and $t = 60$ min with: (a) 7% carbon addition; (b) 14% carbon addition; and (c) 7% carbon + 5% LLDPE addition.

The EDS measured compositions of phases in the samples from the reduction experiments are summarized in Table 2. The composition measurements show that the metals were mainly comprised of iron with Si, Ti, P, S, and V as main trace elements, while the slags were dominated by Na_2O , Al_2O_3 , SiO_2 , CaO , and TiO_2 .

Table 2. EDS measured compositions (in wt.%) of phases in samples from the high-temperature reduction of red mud.

No	Sample	Phases	Fe*/ FeO	Si*/ SiO ₂	Al*/ Al ₂ O ₃	Na*/ Na ₂ O	Ca*/ CaO	Ti*/ TiO ₂	P*/ P ₂ O ₅	S*/ SO ₃	V*/ V ₂ O ₅
1	T = 1400 °C, t = 15 min, 7% carbon	Metal*	99.2	0.00	0.00	0.05	0.02	0.13	0.29	0.19	0.16
		Slag	0.46	40.1	35.3	9.8	8.3	5.6	0.00	0.47	0.00
2	T = 1400 °C, t = 30 min, 7% carbon	Metal*	99.0	0.21	0.13	0.05	0.12	0.00	0.12	0.35	0.00
		Slag	2.5	37.8	35.9	10.1	7.4	5.4	0.26	0.16	0.45
3	T = 1400 °C, t = 60 min, 7% carbon	Metal*	98.5	0.10	0.09	0.00	0.48	0.00	0.36	0.19	0.32
		Slag	3.5	36.2	36.5	9.9	7.7	5.6	0.21	0.28	0.03
4	T = 1450 °C, t = 15 min, 7% carbon	Metal*	98.8	0.13	0.08	0.00	0.03	0.00	0.68	0.31	0.00
		Slag	1.80	36.7	37.0	10.4	7.6	5.6	0.19	0.18	0.41
5	T = 1450 °C, t = 30 min, 7% carbon	Metal*	97.7	0.35	0.06	0.09	0.00	0.19	0.66	0.14	0.84
		Slag	0.88	38.4	37.2	10.6	7.2	5.1	0.22	0.19	0.25
6	T = 1450 °C, t = 60 min, 7% carbon	Metal*	96.7	0.68	0.41	0.22	0.02	0.10	1.01	0.33	0.54
		Slag	0.42	39.6	38.2	10.5	6.6	4.1	0.43	0.07	0.00
7	T = 1500 °C, t = 15 min, 7% carbon	Metal*	96.0	0.51	0.10	0.07	0.01	0.51	0.50	0.21	2.1
		Slag	0.31	38.8	39.3	9.5	6.5	4.9	0.02	0.41	0.09
8	T = 1500 °C, t = 30 min, 7% carbon	Metal*	96.7	0.92	0.00	0.00	0.03	0.56	0.53	0.11	1.19
		Slag	0.51	38.9	38.4	9.9	6.9	4.9	0.27	0.24	0.00
9	T = 1500 °C, t = 60 min, 7% carbon	Metal*	96.5	1.95	0.10	0.00	0.05	0.65	0.25	0.05	0.40
		Slag	0.61	40.1	36.8	7.4	8.4	5.9	0.25	0.12	0.35
10	T = 1450 °C, t = 60 min, 14% carbon	Metal*	79.8	19.1	0.13	0.09	0.05	0.29	0.26	0.02	0.23
		Slag	0.51	36.7	38.6	0.21	23.1	0.16	0.04	0.67	0.00
		Al ₂ O ₃	0.32	0.00	99.1	0.00	0.18	0.06	0.20	0.00	0.10
11	T = 1450 °C, t = 60 min, 7% carbon + 5% LLDPE	Metal*	98.3	0.41	0.07	0.08	0.02	0.44	0.51	0.09	0.08
		Slag	0.60	38.7	36.7	9.8	7.4	5.9	0.00	0.26	0.63

Note: Metal* = elemental composition; Slag and Al₂O₃ = oxide composition.

At 7% carbon addition, the experimental results showed that the metal product was already formed from the red mud even at the lowest temperature of 1400 °C and the shortest time of 15 min. The minor element concentrations in the metal did not show a clear correlation with reduction temperature and time due to their low concentrations and the limitation of the present EDS measurement. The only noticeable correlations were found between the silicon concentration in the metal and the reduction time for reduction temperature of 1500 °C and the silicon concentration in the metal and the reduction temperature for reduction time of 60 min, as shown in Figure 4a. At 1500 °C, the silicon in metal increased with increasing reduction time. For reduction time of 60 min, the silicon in metal also increased with increasing reduction temperature. The increasing silicon in metal indicates an increasing reduction extent of the red mud. The slag compositions from reduction at different temperatures and times are summarized in Figure 4b. The slag from reduction at 1400 °C contained higher residual iron oxide (up to 3.5 wt.%) than the slags from reduction at higher temperatures.

Figure 5 shows the effect of carbon and LLDPE additions at T = 1450 °C on the metal and slag compositions. Increasing the carbon addition from 7% to 14% significantly increased Si content in metal from 1.95 wt.% to 19.1 wt.%. The increase in carbon addition from 7% to 14% also significantly decreased Na₂O in slag from 7.4 wt.% to less than 0.1 wt.%. The Na₂O in the slag was reduced to Na metal by the excess carbon, and the resulting Na metal was then vaporized due to its low boiling point of 882.8 °C. Finally, the decrease of SiO₂ into Si in metal and the removal of Na₂O into volatile Na resulted in the stabilization of solid Al₂O₃, as shown in Figure 3b.

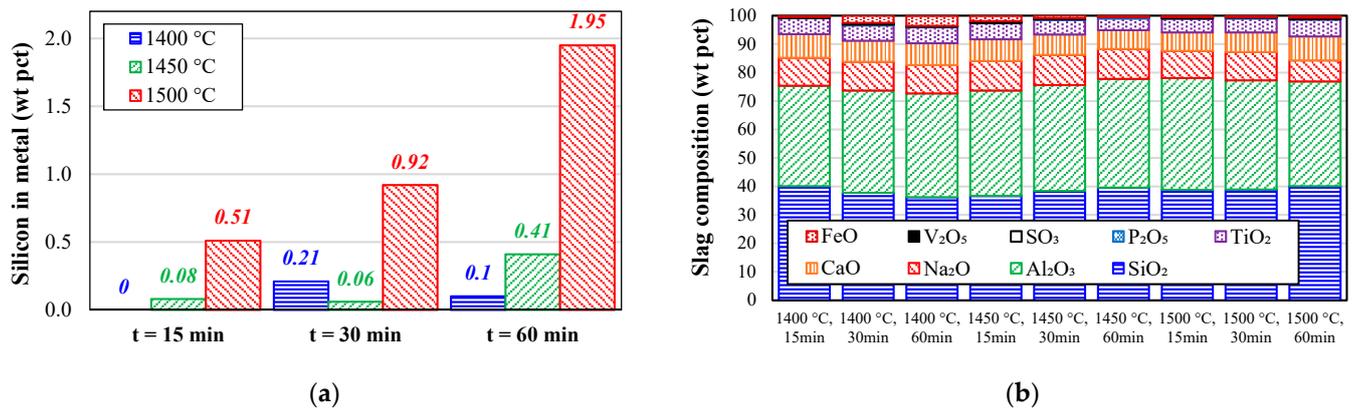


Figure 4. The effects of temperature and time at 7% carbon addition on (a) silicon in metal; and (b) slag composition.

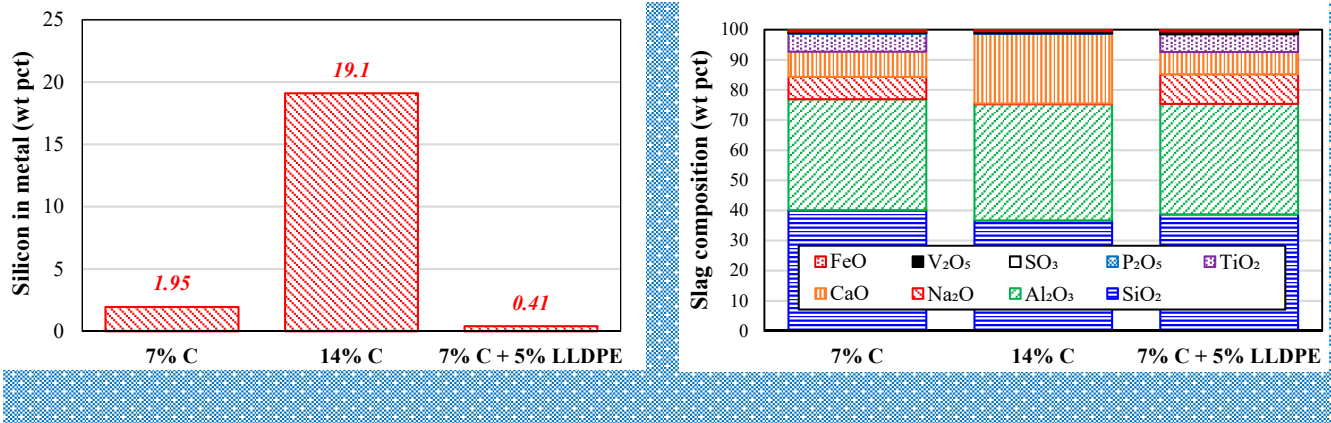


Figure 5. The effects of carbon and LLDPE additions at $T = 1450\text{ }^{\circ}\text{C}$ and $t = 60\text{ min}$ on: (a) Silicon in metal; and (b) Composition of slag.

The experiment with 7% carbon + 5% LLDPE addition gave similar metal and slag characteristics to those from the experiment with only 7% carbon addition. It appears that the LLDPE was combusted at a temperature below $1450\text{ }^{\circ}\text{C}$. The LLDPE was entirely consumed before the reduction process took place, and thus the reduction occurred mainly by the carbon reductant.

The present study shows that the metallic product can be produced by reducing red mud. Fully molten slag can be obtained without the addition of flux when carbon is added at its stoichiometrical requirement. The addition of carbon above its stoichiometrical requirement may promote the formation of a solid Al_2O_3 phase.

4. Conclusions

Thermodynamic analysis and laboratory-scale experiments have been performed to study the reduction of red mud between 1400 and $1500\text{ }^{\circ}\text{C}$. The thermodynamic evaluation shows that the red mud reduction at low-temperature results in a reduction product consisting of spinel, nepheline, and $\text{Na}_2\text{Ca}_3\text{Al}_{16}\text{O}_{28}$ solids. At above $1300\text{ }^{\circ}\text{C}$, the thermodynamical calculation indicates that the reduction product consists of liquid iron and molten slag. At 7% carbon addition, the experimental results show that metal product was generated from reducing red mud at all temperatures and times. The silicon in metal was found to increase with increasing reduction time and increasing reduction temperature. The slags were dominated by Na_2O , Al_2O_3 , SiO_2 , CaO , and TiO_2 , with the highest iron oxide residual found in the slag from reduction at $1400\text{ }^{\circ}\text{C}$. At $1450\text{ }^{\circ}\text{C}$, increasing the carbon addition from 7% to 14% significantly raised the Si content in metal from 1.95 wt.%

to 19.1 wt.% and significantly decreased Na₂O in slag from 7.4 wt.% to less than 0.1 wt.%. The LLDPE did not significantly contribute to the reduction process due to its elimination by combustion before the reduction process.

Author Contributions: Conceptualization, Z.Z. and T.H.; methodology, L.G. and T.H.; formal analysis, L.G. and T.H.; investigation, L.G. and T.H.; resources, Z.Z. and T.H.; data curation, L.G. and T.H.; writing—original draft preparation, L.G. and T.H.; writing—review and editing, L.G., Z.Z. and T.H.; visualization, L.G. and T.H.; supervision, Z.Z. and T.H.; project administration, T.H.; funding acquisition, T.H. All authors have read and agreed to the published version of the manuscript.

Funding: This research was funded by The Asahi Glass Foundation.

Institutional Review Board Statement: Not applicable.

Informed Consent Statement: Not applicable.

Data Availability Statement: Data is contained within the article.

Acknowledgments: The authors would like to thank PT. Indonesia Chemical Alumina (ICA) for providing materials used for experiments.

Conflicts of Interest: The authors declare no conflict of interest.

References

1. Power, G.; Gräfe, M.; Klauber, C. Bauxite residue issues: I. Current management, disposal and storage practices. *Hydrometallurgy* **2011**, *108*, 33–45. [\[CrossRef\]](#)
2. Balomenos, E.; Gianopoulou, I.; Panias, D.; Paspaliaris, I. A novel red mud treatment process: Process design and preliminary results. *Trav. ICSOBA* **2011**, *36*, 255–266.
3. Balomenos, E.; Gianopoulou, I.; Panias, D.; Paspaliaris, I. A novel red mud treatment process. In Proceedings of the 3rd International Conference on Industrial and Hazardous Waste Management, Chania, Greece, 12–14 September 2012; pp. 1–7.
4. Balomenos, E.; Giannopoulou, I.; Gerogiorgis, D.; Panias, D.; Paspaliaris, I. Resource-efficient and economically viable pyrometallurgical processing of industrial ferrous by-products. *Waste Biomass Valorization* **2013**, *5*, 333–342. [\[CrossRef\]](#)
5. Balomenos, E.; Kastritis, D.; Panias, D.; Paspaliaris, I.; Boufounos, D. The ENEXAL bauxite residue treatment process: Industrial scale pilot plant results. *Light Met.* **2014**, 143–147. [\[CrossRef\]](#)
6. Balomenos, E.; Davris, P.; Pontikes, Y.; Panias, D.; Delipaltas, A. Bauxite residue handling practice and valorisation research in aluminium of Greece. In Proceedings of the 2nd International Bauxite Residue Valorisation and Best Practices Conference, Athens, Greece, 7–10 May 2018; pp. 29–37.
7. Chun, T.; Li, D.; Di, Z.; Long, H.; Tang, L.; Li, F.; Li, Y. Recovery of iron from red mud by high-temperature reduction of carbon-bearing briquettes. *J. South. Afr. Inst. Min. Metall.* **2017**, *117*, 361–364. [\[CrossRef\]](#)
8. Guo, Y.H.; Gao, J.J.; Xu, H.J.; Kai, Z.H.A.O.; Shi, X.F. Nuggets production by direct reduction of high iron red mud. *J. Iron Steel Res. Int.* **2013**, *20*, 24–27. [\[CrossRef\]](#)
9. Valeev, D.; Zinoveev, D.; Kondratiev, A.; Lubyanoi, D.; Pankratov, D. Reductive Smelting of Neutralized Red Mud for Iron Recovery and Produced Pig Iron for Heat-Resistant Castings. *Metals* **2020**, *10*, 32. [\[CrossRef\]](#)
10. Wang, K.; Liu, Y.; Lyu, G.; Li, X.; Chen, X.; Zhang, T. Recovery of Iron from High-Iron Bayer Red Mud by Smelting Reduction. *Light Met.* **2020**, 92–97. [\[CrossRef\]](#)
11. Pera, J.; Boumaza, R.; Ambroise, J. Development of a pozzolanic pigment from red mud. *Cem. Concr. Res.* **1997**, *27*, 1513–1522. [\[CrossRef\]](#)
12. Sglavo, V.M.; Campostrini, R.; Maurina, S.; Carturan, G.; Monagheddu, M.; Budroni, G.; Cocco, G. Bauxite ‘red mud’ in the ceramic industry. Part 1: Thermal behavior. *J. Eur. Ceram. Soc.* **2000**, *20*, 235–244. [\[CrossRef\]](#)
13. Altundogan, H.S.; Altundogan, S.; Tumen, F.; Bildik, M. Arsenic adsorption from aqueous solutions by activated red mud. *Waste Manag.* **2002**, *22*, 357–363. [\[CrossRef\]](#)
14. Srikanth, S.; Ray, A.K.; Bandopadhyay, A.; Ravikumar, B. Phase constitution during sintering of red mud and red mud-fly ash mixtures. *J. Am. Ceram. Soc.* **2005**, *88*, 2396–2401. [\[CrossRef\]](#)
15. Vachon, P.; Tyagi, R.D.; Auclair, J.C.; Wilkinson, K.J. Chemical and biological leaching of aluminum from red mud. *Environ. Sci. Technol.* **2005**, *28*, 26–30. [\[CrossRef\]](#) [\[PubMed\]](#)
16. Snars, K.; Gilkes, R.J. Evaluation of bauxite residues (red muds) of different origins for environmental applications. *Appl. Clay Sci.* **2009**, *46*, 13–20. [\[CrossRef\]](#)